Article

Structure-directed functional properties of phenothiazine brominated dyes. Morphology, photophysical and electrochemical properties

Andrei Bejan, Sergiu Shova, Mariana Dana Damaceanu, Bogdan C Simionescu, and Luminita Marin

Cryst. Growth Des., **Just Accepted Manuscript** • DOI: 10.1021/acs.cgd.6b00212 • Publication Date (Web): 24 May 2016

Structure-directed functional properties of phenothiazine brominated dyes. Morphology, photophysical and electrochemical properties

Andrei Bejan, Sergiu Shova, Mariana Dana Damaceanu, Bogdan C. Simionescu and Luminita Marin*

"Petru Poni" Institute of Macromolecular Chemistry of Romanian Academy, Iasi, Romania

lmarin@icmpp.ro

Abstract

A series of nine dyes based on electron-donating phenothiazine core functionalized with various carbonyl containing electron-withdrawing moieties as primary end group and with or without bromine as a second heavy end group, were designed and synthesized to generate variable supramolecular architectures with distinct thermotropic, photophysical and electrochemical properties. The supramolecular architecture of the obtained dyes was studied in detail by single crystal X-ray diffraction and polarized light microscopy, while optoelectronic properties were investigated by UV-vis and photoluminescence spectroscopy and cyclic voltammetry measurements. The phenothiazine dyes emit light from UV to orange domain, depending on the electron-withdrawing substituent, with great quantum yield reaching up to 71 % and high color purity. The introduction of the bromine as a second substituent produced nearly the twofold increase of the quantum yield, compared to their counterparts. It was settled that this major benefit of the bromine on the improvement of the quantum yield happened, due to the fact that by its presence some molecular orbital interactions were generated. An interesting and challenging achievement was evidenced in the case of the direct connection of the formyl group to the phenothiazine ring when an unexpected planarization of the dye, unknown up to now in the literature, with drastic consequences on the photophysical and electrochemical behavior was attained. It was concluded that there is a close relationship between the nature of the building blocks of the phenothiazine dyes and their ability to promote favorable properties for different optoelectronic applications.

1. Introduction

Use of organic materials as active substrate in building electronic and optoelectronic devices captured growing interest in development of highly conjugated compounds with efficient

performances. Compared to their inorganic counterparts, organic materials bring great advantages: are cheaper, environmentally safer and easily amenable for modulation. Supramolecular organization capability of the small molecules enables higher charge carrier mobility compared to polymeric semiconductors with large amorphous fractions. Hence, developments of low molecular weight compounds and further understanding the relationship between structure and properties are of crucial importance and still remain challenging to the scientific community. Among organic compounds, those based on (hetero)aromatic π-conjugated systems end-capped with an electron donor and electron-acceptor giving donor-acceptor chromophores proved significant broader opportunities [1].

Phenothiazine – a fused heteroaromatic ring attracted a special attention in view of use as active substrate in electronic and optoelectronic devices. Due to the presence of rich electron sulfur and nitrogen atoms, phenothiazine has a strong electron-donating feature and hence ability to promote extended conjugation. Some phenothiazine based compounds proved high carrier mobility and low emission properties being used in building photovoltaics [2-5] or field effect transistor [6-8], while others proved high luminescence and moderate mobility giving organic light emission diodes with good performances [9-16]. The balance of properties which guides the material to the applications is a function of the intrinsic properties but also of the supramolecular arrangement. Even if a plenty of phenothiazine based materials were synthesized and used in testing for above mentioned optoelectronic devices, only for a few the supramolecular structure was reported [17-22]. They revealed that phenothiazine ring adopts a bent structure known as butterfly geometry, which further promotes a supramolecular architecture with large intermolecular distances of the compounds containing it. In this way, the non-radiative decay is hindered, and thus good luminescence in solid state is preserved, making compounds containing it promising candidates for organic light emitting diodes.

On the other hand, the efforts drained in the direction of luminescence improving of organic compounds, recently revealed that compounds functionalized with carbonyl and bromine moieties have an amazing increase of luminescence quantum yield even for simple rigid chromophore units [23-25].

In this context, the present paper reports a systematic study on a large series of nine donor-acceptor phenothiazine dyes functionalized with heavy bromine atom and/or electron-acceptor carbonyl groups as formyl, carboxyl and cyanoacrylic acid moieties. Six of them were

successfully grown as single crystals. The study is related to the supramolecular packing, photophysical and electrochemical characteristics of the obtained donor-acceptor dyes, with a special concern on the understanding the structure - properties relationship and the role of bromine on electronic structure and photophysical properties. It should be stressed that the systematic and detailed study from morphological, optical and electrochemical point of view of a large series of phenothiazine derivatives is reported here for the first time.

2.1. Experimental

Materials

Iodophenol 99%, *n*-bromohexane 98%, phenothiazine 98%, cyano acetic acid 99%, copper powder 99.9%, phosphorous oxychloride 99%, *N*-bromosuccinimide 99% and dimethylformamide 99.8% were purchased from Aldrich and used as received. 18-Crown-6 99% from Fluka and piperidine 99.5% from Acros Organics were used without any further purification. All the solvents of high purity used in this study were purchased from Aldrich and used as received.

Synthesis

All the syntheses were performed with an input from literature data [29-34] and optimized to reach the best reaction yield. Synthetic procedure and structural characterization by NMR, FTIR and elemental analysis is provided in supplementary information section.

Crystal growth

Taking into consideration the chemical structure of the new synthesized dyes, more specifically the presence of the aliphatic tails and the rigid aromatic core with donor-acceptor character conferring polarity and ability to develop H-bonds or π-π interactions, conditions for their growth as single crystals were designed. To favor the polar-nonpolar segregation, polar solvents containing aliphatic parts as ethanol, acetonitrile or ethyl acetate were used. Anticipating non-coplanar structure of the dyes and so difficult ordering, solvents with higher boiling points along with dye size increasing have been chosen, in order to avoid fast evaporation and thus to slowly change the concentration in the nucleation area. The compounds were dissolved into the solvent under the oversaturation concentration, and the solution was kept in seals covered with aluminium foils with few punched holes. This strategy worked well for 6 of the synthesized dyes, for each large single crystal proper for X-ray diffraction being grown.

Equipment

Infrared spectra were recorded on a FT-IR Bruker Vertex 70 Spectrophotometer in the transmission mode, by using KBr pellets.

The NMR spectra were obtained on a Bruker Avance DRX 400 MHz Spectrometer equipped with a 5 mm QNP direct detection probe and z-gradients. The spectra have been recorded in DMSO-d_6, at room temperature. The chemical shifts are reported as δ values (ppm) relative to the residual peak of the solvent.

Crystallographic measurements of the compounds (2), (4), (5), (6), and (9) were carried out with an Oxford-Diffraction XCALIBUR E CCD diffractometer equipped with graphite-monochromated Mo Kα radiation. Single crystals were positioned at 40 mm from the detector and 467, 353, 248, 388, and 464 frames were measured each for 30, 25, 10, 30, and 15 s over 1° scan width. The X-ray data for (7) were collected using an Agilent SuperNova dual wavelength X-ray diffractometer using Cu Kα radiation. The crystal was positioned at 46 mm from the detector and 1781 frames were measured each for 2-8 s over 1° scan width. The unit cell determination and data integration were carried out using the CrysAlis package of Oxford Diffraction [35]. All the structures were solved by direct methods using Olex2 [36] software with the SHELXS structure solution program and refined by full-matrix least-squares on F^2 with SHELXL-97 [37]. Atomic displacements for non-hydrogen atoms were refined using an anisotropic model. Hydrogen atoms have been placed in fixed, idealized positions accounting for the hybridization of the supporting atoms and the possible presence of hydrogen bonds in the case of donor atoms. The molecular plots were obtained using the Olex2 program. The positional parameters of the disordered hexyl fragment in (4) and –CH=O and Br atoms in (6) were refined in combination with PART and SADI restrains using anisotropic/isotropic model for non-H atoms. Table 1s provides a summary of the crystallographic data together with refinement details for studied compounds. CCDC 1414998 for (2), 1414934 for (4), 1414933 for (5), 1414156 for (6), 1415271 for (7) and 1415052 for (9) contain the supplementary crystallographic data for this contribution. These data can be obtained free of charge from the Cambridge Crystallographic Data Centre via www.ccdc.cam.ac.uk/data_request/cif

The thermotropic behavior of the dyes was investigated with an Olympus BH-2 polarized light microscope under cross polarizers equipped with a THMS 600 hot stage and a LINKAM TP92 temperature control system.

UV–Vis absorption and photoluminescence spectra were recorded on a Carl Zeiss Jena SPECORD M42 spectrophotometer and a Perkin Elmer LS 55 spectrophotometer, respectively, in solution (10^{-5} M), using 10 mm quartz cells. The fluorescence quantum yield (Φ_F) of the samples was measured on a FluoroMax-4 spectrofluorometer equipped with a Quanta-phi integrating sphere accessory Horiba Jobin Yvon, at room temperature. The solution concentration was optimized to obtain an absorbance around 0.055. The slit widths and detector parameters were optimized to maximize but not saturate the excitation Rayleigh peak, in order to obtain a good optical luminescence signal-to-noise ratio.

Electrochemical properties were investigated by cyclic voltammetry (CV) carried out on a Potentiostat-Galvanostat (PG581, Uniscan Instruments). The electrochemical cell was equipped with three-electrodes: a working electrode (ITO-coated glass slide), an auxiliary electrode (platinum wire) and a reference electrode (calomel-SCE). Tetrabutylammonium perchlorate /dichloromethane was used as a supporting electrolyte system. The measurements were registered for the solution dyes having the same concentration, of 1×10^{-3} M. All potentials were reported with respect to calomel (SCE) electrode under ambient conditions, at the scan rate of 100 mV/s. Ferrocene/ferrocenium (F_c/F_c^+) redox standard was used as an external reference for calibration (+0.45 *vs* SCE). The oxidation and reduction onset potentials were determined at the intercept of the two tangents drawn at the rising current and baseline charging current of the CV curves.

3. Results and discussions

Design, synthesis, structural and supramolecular characterization

A series of nine phenothiazine dyes functionalized with bromine and/or different electron-withdrawing units containing carbonyl moiety were designed and synthesized according to the Scheme 1. The phenothiazine has been chosen as a central core, taking into consideration its strong electron-donor character which facilitates the electron delocalization and promotes high quantum yield [20, 38-41]. To improve more its donating ability, the phenothiazine was substituted with *N*-hexyloxy-phenylene unit [26-28, 42, 43]. The resulted phenothiazine core was functionalized with carbonyl containing moieties having different electron-accepting ability, in order to create donor-acceptor (D-A) systems and to enhance the emission capability, as well. Thus, the good electron delocalization and the low band gap create the premises of a good mobility of the charge carriers. The acceptor units have different withdrawing power to give rise

different band gaps and thus to tune the color of the emitted light. Targeting a high quantum yield, a heavy bromine group has been introduced as a second substituent to promote the halogen bonding probability and thus to activate efficient luminescence of the resulted pure organic materials [26-28, 44-46].

The phenothiazine core has been prepared by Ullmann reaction of phenothiazine with *n*-hexyloxy-4-iodobenzene, using 18-crown-6 ether as phase transfer catalyst [29], the *n*-hexyloxy-4-iodobenzene being obtained via Williamson etherification of 4-iodo-phenol with *n*-bromohexane [30]. The formyl substituent was grafted on the phenothiazine core *via* Vilsmeier-Haak reaction [31] and the obtained aldehyde was transformed into (i) cyanoacrylic derivative *via* Knovenagel condensation reaction [32], and (ii) carboxyl unit *via* oxidation of the formyl group [33]. The bromine derivatives were obtained using *N*-bromosuccinimide reagent [29, 34]. All the synthetic procedures were optimized to attain the best reaction yield. The obtained compounds have good solubility in common organic solvents such as acetonitrile, tetrahydrofuran, chloroform or dichloromethane, which allowed their easy characterization.

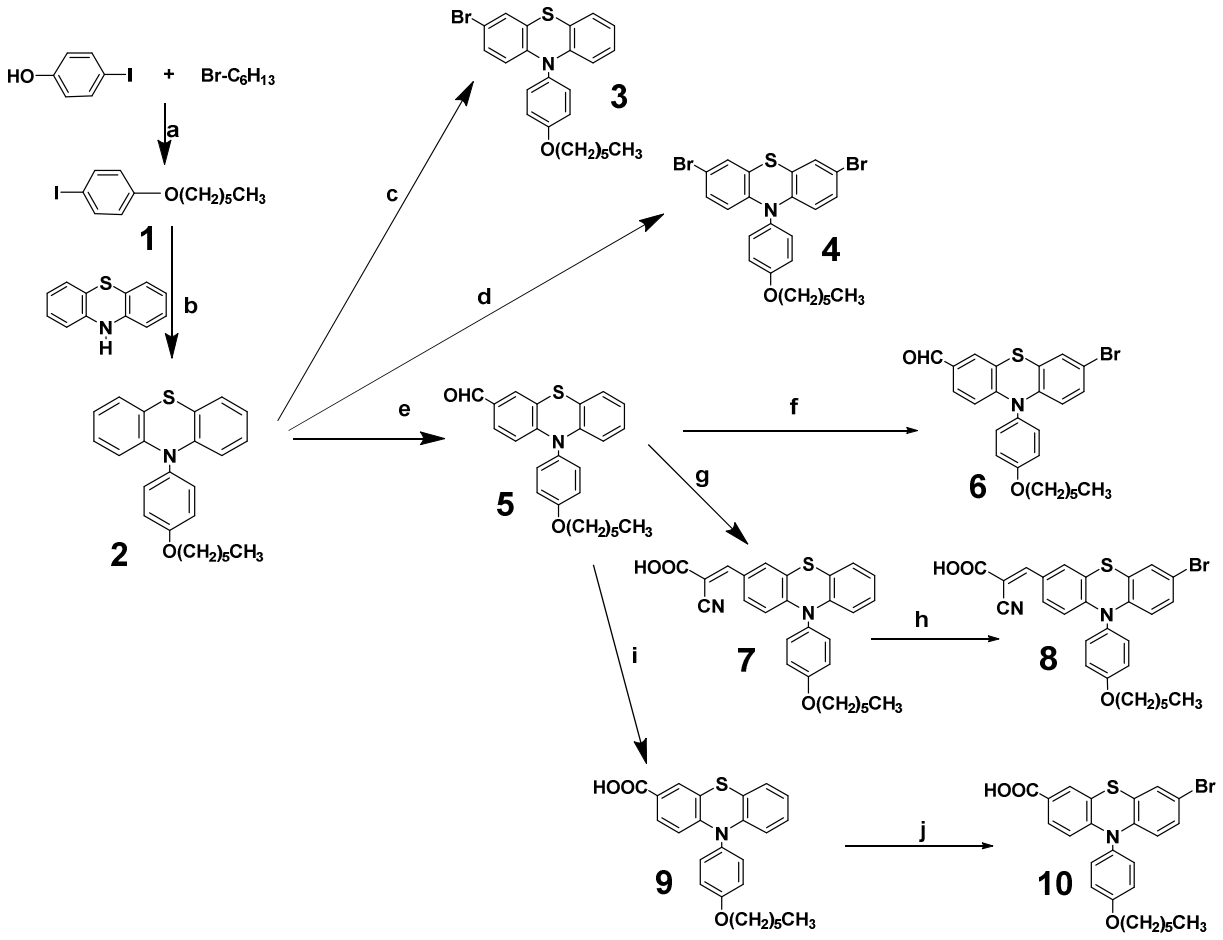

Scheme 1. Phenothiazine derivatives synthesis: (a) DMF, K_2CO_3, 110-120 °C, 8h; (b) *o*-diclorbenzene, copper powder, 18-crown-6, K_2CO_3, 168 °C, 24h; (c), (d), (f), (h) NBS, $CHCl_3$, CH_3COOH, 0 °C, 2h; (e) DMF, $POCl_3$, $C_2H_4Cl_2$, 90 °C, 24h; (g) cyanoacetic acid, piperidine, acetonitrile, 80°C, 24h; (i) THF, *t*-BuOK, 0 °C, RT, 24h; (j) NBS, DMF, 0 °C, 2h.

The synthetic pathway was firstly confirmed by FTIR spectra by the appearance of the main absorption bands due to the phenothiazine parent molecule (2) as: stretching of the aromatic C-H bonds (3095 – 3043 cm^{-1}) and methylene and methyl units (2954 – 2850 cm^{-1}); stretching of the C=C of the aromatic units (1607 – 1467 cm^{-1}); deformation of the aromatic rings (838 – 744 cm^{-1}); stretching of the ether unit (1245 – 1237 cm^{-1}). The newly formed moieties were evidenced by specific group vibration bands: the C=O (1725 – 1662 cm^{-1}), C-Br (1167 – 1027 cm^{-1}) or C≡N (2219 cm^{-1}). Further, the structure of the synthesized compounds has been confirmed by ^{1}H-NMR spectra – which showed the chemical shifts of the all protons in the right integral ratio, and ^{13}C-NMR spectra (Figures 1s-10s) and elemental analysis.

Apart from the above mentioned investigations, the crystal structure of the dyes under study, except (3, 8 and 10), confirmed the targeted molecular structure and provided relevant information about the nature of the intermolecular interactions and packing peculiarities, which were further correlated with their properties. The results of the single crystal X-ray study, along with the atom labelling scheme, are shown in Figure 1. Bond distances and angles are summarized in Table 1S.

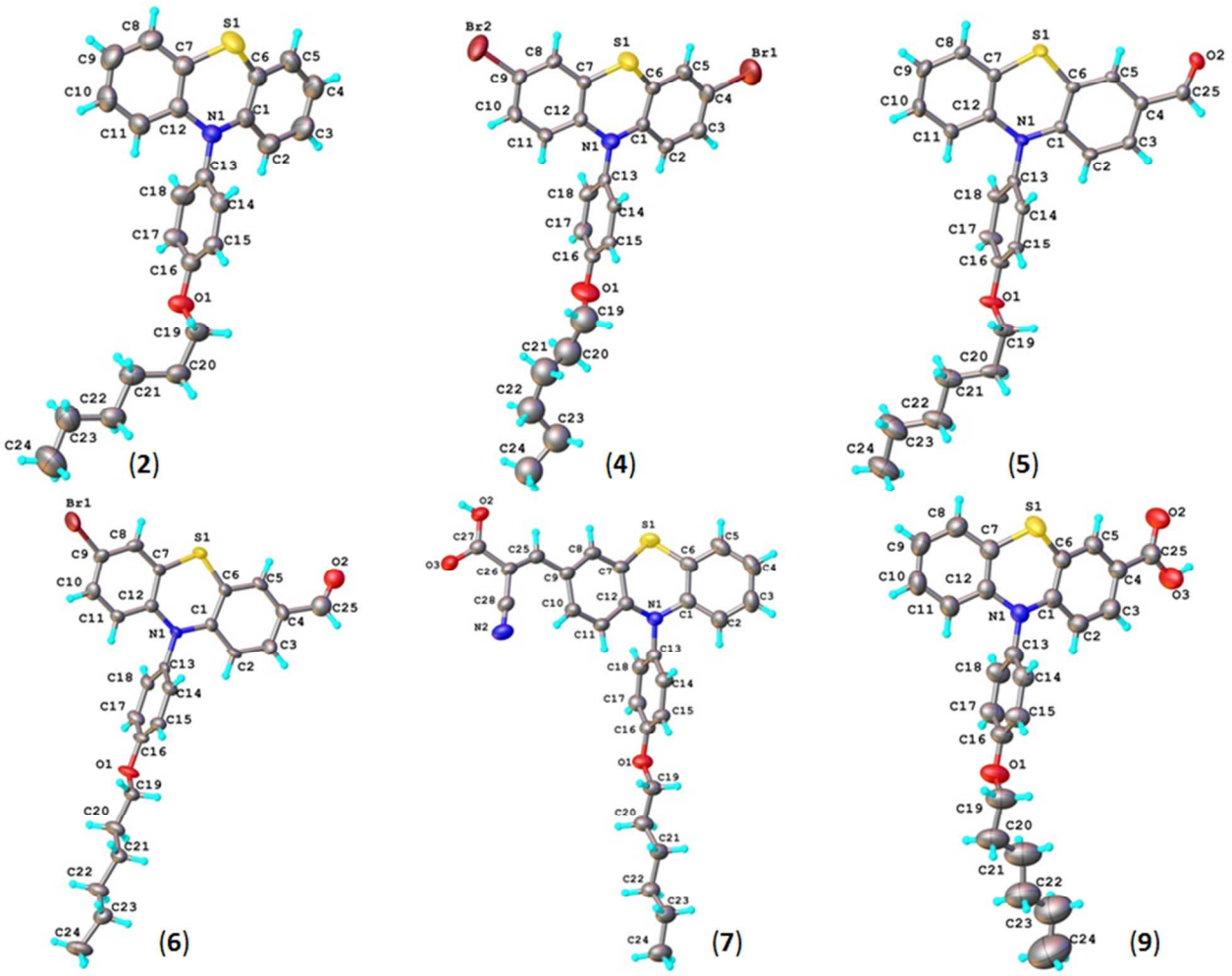

Figure 1. X-ray molecular structure of the compounds under study

As can be seen, there are no solvate molecules in the crystals of the studied compounds. The X-ray structural investigation has demonstrated that all the compounds exhibit close molecular geometry which is in a good agreement with the values of earlier studied phenothiazine derivatives [17-25, 31]. Thus, the mean value of the C-S bond lengths is 1.756 ± 0.021 Å and that of the C-N bond lengths within the central ring is 1.427 ± 0.039 Å. The mean values of the C-S-C is 100.60 + 3.38°, while C1-N1-C12, C1-N1-C13 and C12-N1-C13 bond angles are of 123.21 ± 1.88°, 117.60 ± 0.50° and 117.72 ± 0.98°, respectively. Similar molecular conformations were observed for all the structures.

Analysing the planar fragments, one can be concluded that as a whole, similar conformations are observed for all the structures in the crystal. The oxyphenyl ring is almost perpendicular to the mean plane of the phenothiazine fragment. The dihedral angle between this

ring and bisectral plane of the phenothiazine fragment varied in the range of 1.2°-3.7°, except the derivative containing bromine and formyl substituents (6) for which this angle increased at 11.2°. On the other hand, the phenothiazine core adopted different conformations in the dyes. In four of them, namely (2), (4), (7) and (9), the phenothiazine system is folded along S1···N1 vector, with the dihedral angles between the two benzene rings of 156.2°, 157.9°, 144.8° and 155.6° respectively, giving the well-known butterfly conformation [17-25]. These values falls in the range of those earlier found for N-substituted phenothiazine derivatives [17-25]. On the contrary, the analogue dihedral angle in the phenothiazine fragment of the (5) and (6) molecules containing aldehyde group has values of 178.8° and 176.6° respectively, providing evidence of a planar conformation, different from the butterfly one reported up to now for phenothiazine derivatives. Comparing the structures of the (5) and (6) with similar ones reported in literature as having butterfly conformation [23-25], it appeared that the determining role on planarization is played by the phenyl substituent of the nitrogen atom of the phenothiazine. This direct connection increases the electron donor capability of the phenothiazine [26-28, 42, 43] and consequently its ability to conjugate with the donor formyl unit, arising planar conformers.

The different functional groups of the compounds determined a variety of packing modes in the crystals, once again highlighting their importance as building blocks in structural design of the compounds for different applications. Thus, in the crystal structure of the phenothiazine core (2), two crystallographic equivalent molecules are linked to form dimeric units through C-H···O hydrogen bonding, where hexyloxy-phenyl oxygen atom acts as acceptor. A view of this dimeric unit is depicted in Figure 2.

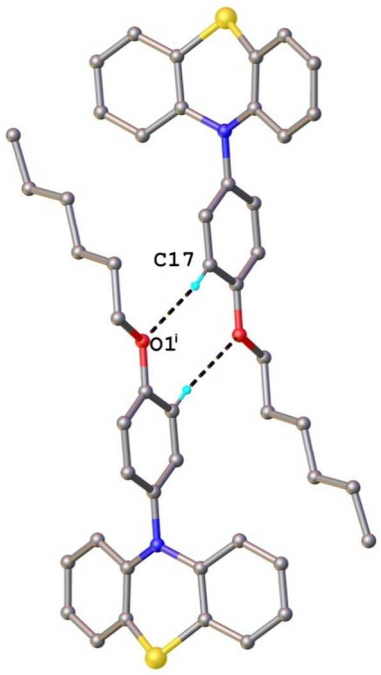

Figure 2. View of the dimeric unit in the crystal structure (2). (Non-relevant H-atoms are omitted for clarity.) H-bonds parameters: C17−H···O1 [C17−H 0.93 Å, H···O1 2.03 Å, C17···O1(2 – *x*, 2 – *y*, 1 – *z*) 2.833(7) Å, O5−H···O1 165.9°].

The carboxyl units of the (7) and (9) dyes proved to be appropriate fragments to play the role of proton-donor and proton-acceptor for a classical O-H···O hydrogen bonding. Thus, in their crystals, the carboxylic groups are involved into formation of a stable cyclic hydrogen bonded system. Consequently, the main crystal packing motif is characterized by a dimeric centrosymmetric associate, as shown in Figures 3a and 3b, respectively. In the crystal, the dimeric units are further extended through short C-H···O or C-H···N intermolecular contacts to form supramolecular ribbons.

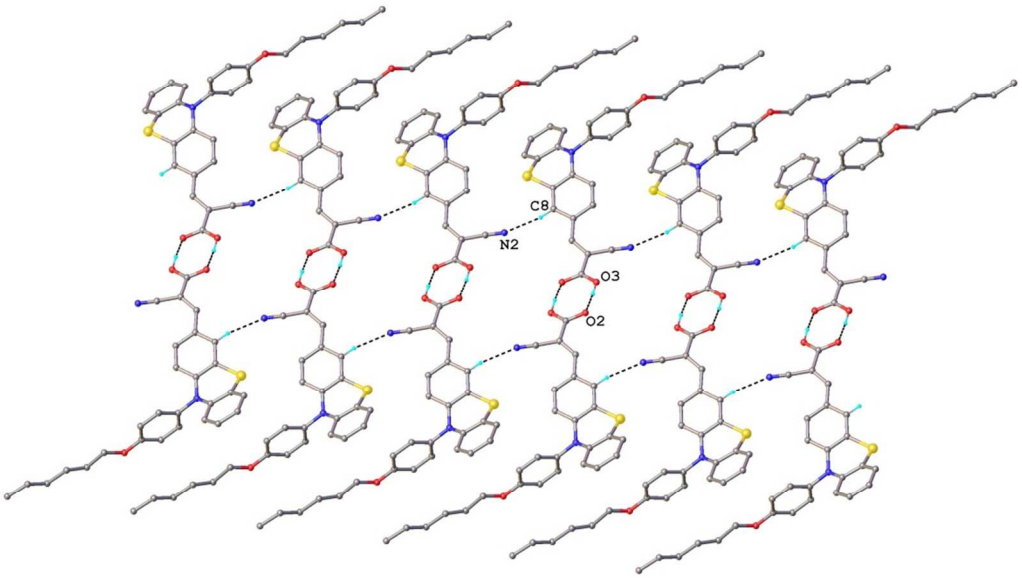

a)

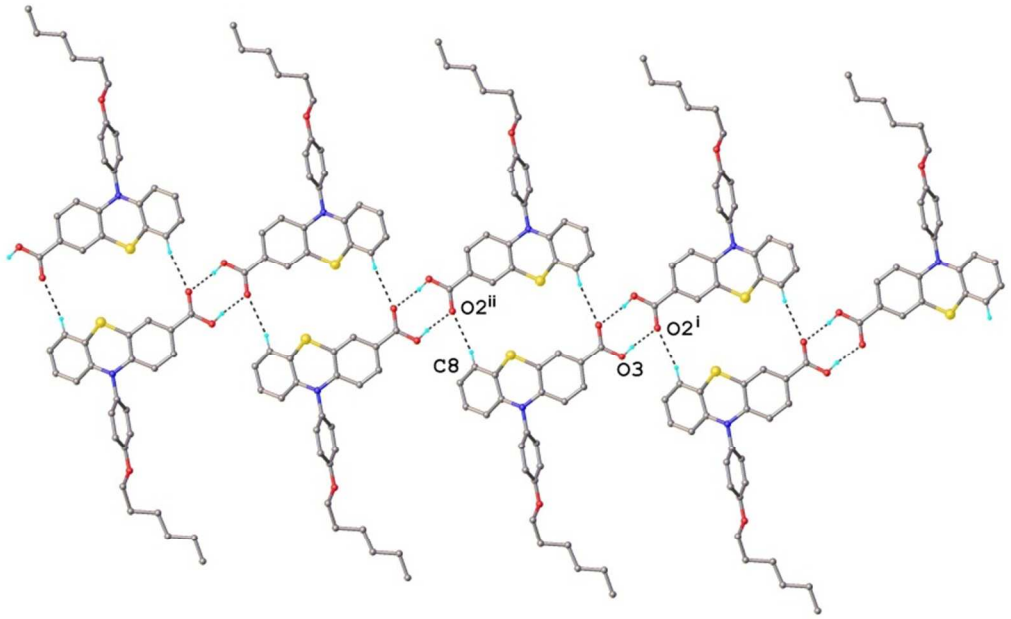

b)

Figure 3. a) View of the dimeric associate in the crystal structure of (7). H-bonds parameters: O3−H···O2 [O3−H 0.82 Å, H···O2 1.90 Å, O3···O2(2 – *x*, –*y*, 2 – *z*) 2.612(2) Å, O3−H···O2 145.3°]; C8−H···N2 [C8−H 0.93 Å, H···N2 2.60 Å, C8···N2(*x* – 1, *y*, *z*) 3.451(3) Å, C8−H···N2 152.8°]. b) A view of a supramolecular ribbon in the crystal structure (9). H-bonds parameters: O3−H···O2 [O3−H 0.82 Å, H···O2 1.79 Å, O3···O2(1 – *x*, 1 – *y*, 1 – *z*) 2.604(2) Å, O3−H···O2 171.8°]; C8−H···O2 [C8−H 0.93 Å, H···O2(1 – *x*, 1 – *y*, 2 – *z*) 2.53 Å, C8···O2 3.442(3) Å, C8−H···O2 167.0°](Non-relevant H-atoms are omitted for clarity.)

The analysis of the crystal structure of the formyl containing compound (5) has shown that the packing of the neutral molecules was driven by the system of C−H···O intermolecular hydrogen bonding resulting into a three-dimensional supramolecular network. The centroid-to-centroid distances of 4.052 Å between benzene rings of centrosymmetrically related phenothiazine moieties evidenced that weak π-π stacking interactions within the network were also present. The view of packing diagram in the crystal structure (5) is depicted in Figure 4.

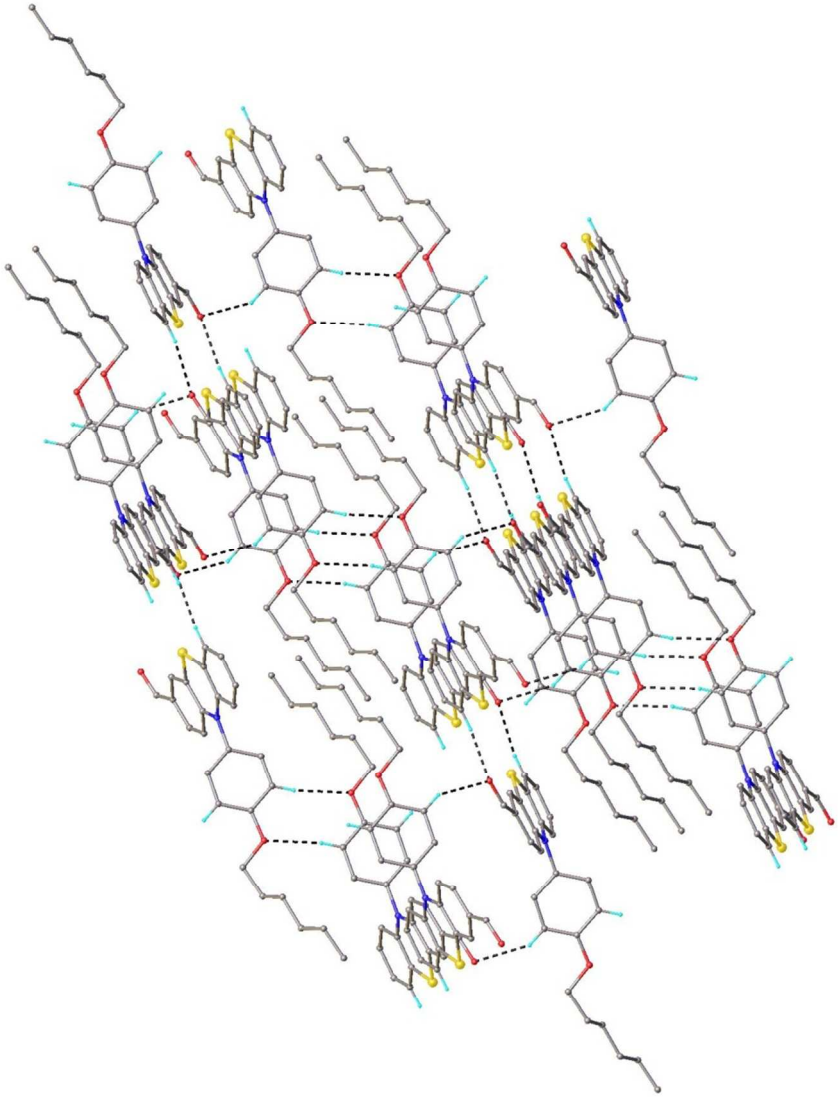

Figure 4. View of the 3D supramolecular architecture in the crystal structure (5). H-bonds parameters: C8−H···O2 [C8−H 0.93 Å, H···O2 2.41 Å, C8···O2(–*x*, –0.5 – *y*, 0.5 – *z*) 3.316(3) Å, C8−H···O2 165.8°]; C17−H···O1 [C17−H 0.93 Å, H···O1 2.51 Å, C17···O1(1 –*x*, –*y*, 2 – *z*) 3.413(3) Å, C17−H···O1 164.7°]; C15−H···O2 [C15−H 0.93 Å, H···O2 2.57 Å, C15···O2(–*x*, –0.5 + *y*, 1.5 – *z*) 3.368(3) Å, C15−H···O2 144.3°].

By introduction of the bromine substituent, the crystal structure of the formyl containing molecule (6) changed, the π-π stacking becoming the driving force responsible for the packing motif. In the crystal structure (6), the neutral molecules are associated to form a linear array due to the system of π-π stacking, as shown in Figure 5. The *Cg*1···*Cg*1(–*x*, –*y*, 2 – *z*) and *Cg*1···*Cg*2(–*x*, 1 – *y*, 2 – *z*) distances are of 3.632 Å and 3.751 Å, respectively, signature of strong π-π stacking interactions. The C9-Br1 distance (1.817(6) Å) is only slight smaller compared to the average C-Br distance (1.88-1.93 Å), or compared to the C-Br distance in the compound (4) (C4-Br1: 1.908(6) Å; C9-Br2: 1.895(6) Å), indicating a weak conjugation with the phenothiazine core due to bromine electronic structure (Figure 1) [47-49].

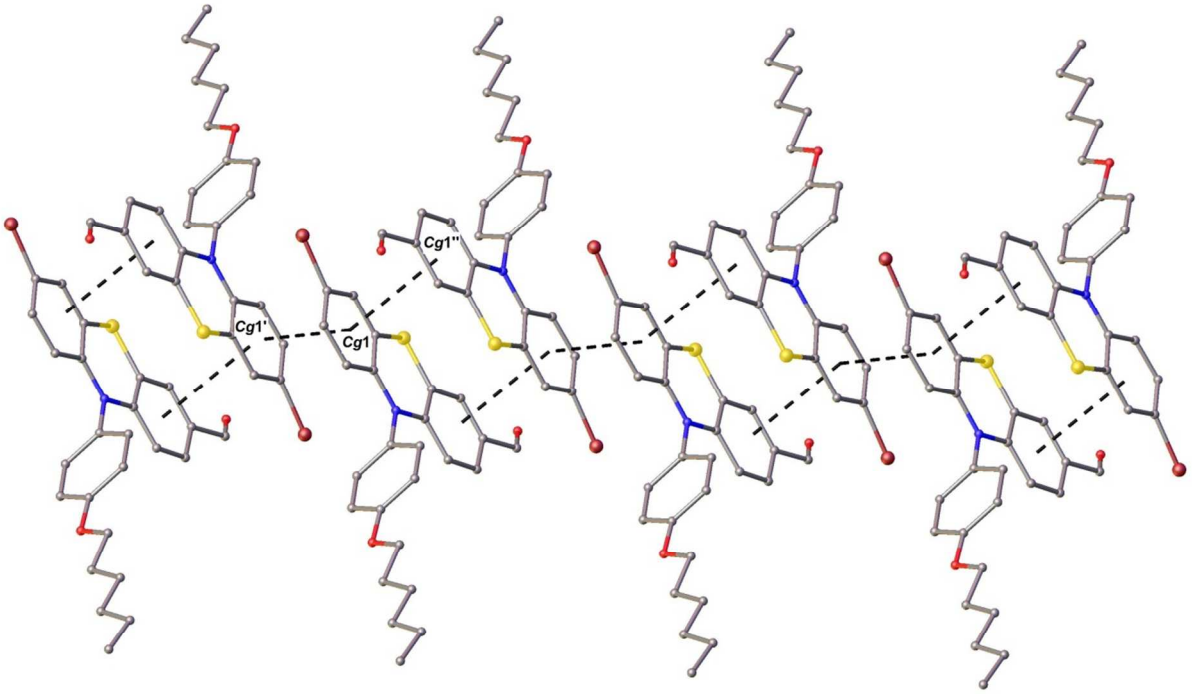

Figure 5. π-π stacking interactions in the crystal structure of (6). Hydrogen atoms are omitted for clarity.

It is important to note, that the planar conformation observed for the phenothiazine fragment of the (5) and (6) molecules appeared as a consequence of the direct connection of the electron-acceptor formyl with electron-donating phenothiazine. This particular donor-acceptor system has produced a strong electron delocalization, affording the planarization of the phenothiazine core and further π-π stacking interactions which were absent in the phenothiazine derivatives reported up to now [17-25]. This is of further interest in choosing building blocks for

the material design addressed to applications which claim good high charge carrier mobility. Analyzing the case of the derivative containing bromine (6) compared with its counterpart (5), one could be observed stronger π-π interactions on a hand (the centroid-to-centroid distances of 3.632 Å and 3.751 Å in the (6) compared to 4.052 Å in the (5)) and lower planarization effect of the phenothiazine core on the other hand (the dihedral angle value in the phenothiazine fragment is 176.6° in the (6) compared to 178.8° in the (5)), indicating the bromine with an own contribution in the self-assembling process.

In the crystal structure of the compound containing two bromine substituents (4) the π-π stacking interaction *Cg*1···*Cg*1(2 -*x*, 2 -*y*, 1 – *z*) of 3.820 Å in combination with the C15-H···*Cg*1(2 -*x*, 2 -*y*, 2 – *z*) contacts of 2.887 Å resulted into the formation of tetrameric clusters as the main crystal packing units (Figure 6). It appeared that the introduction of the bromine substituent favors the π-π stacking interaction of the phenothiazine dyes, creating premises for a good charge transport.

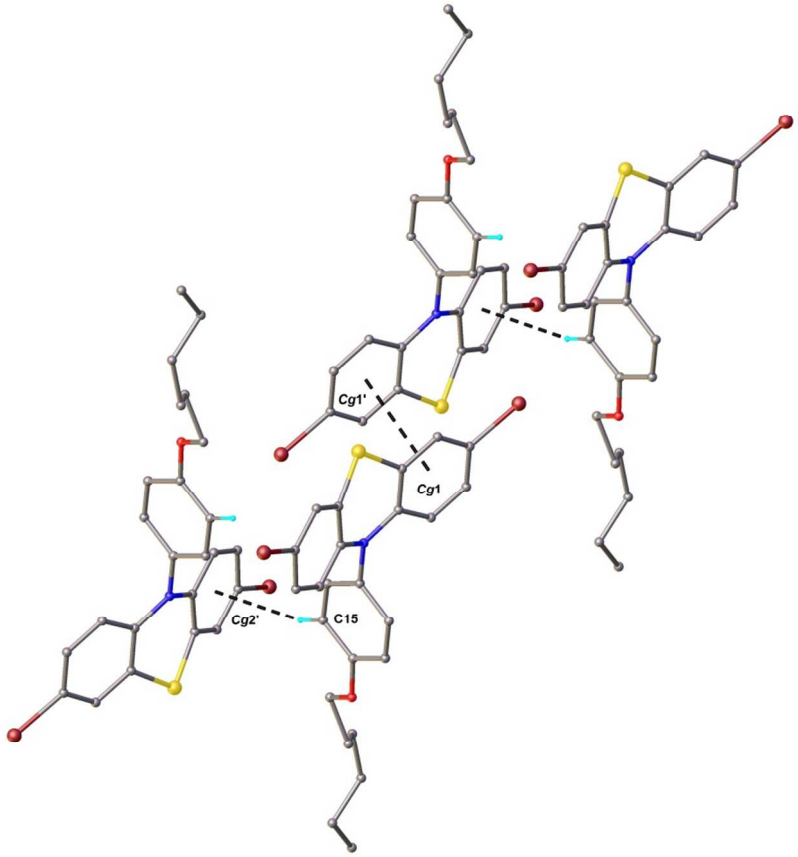

Figure 6. Tetramer supramolecular unit in the crystal structure (4)

Thermotropic behavior

All the obtained dyes exhibited strong birefringence under polarized light microscopy (POM), according to their crystalline nature (Figure 7a, b, c). They melted during the heating and, as expected, the melting point increased once the electron-withdrawing character of the substituent increased resulting in a more extended molecular conjugation which induced longer rigid structures and consequently weaker mobility. The introduction of the bromine as a second substituent increased more the melting point compared to the counterparts without bromine, in agreement with the morphological conclusions which indicated stronger π-π stacking interaction. On the other hand, the crystallization occurred (i) during the cooling only for the compounds (6) and (9), (ii) slowly from the glassy state at room temperature for the compounds (2), (3), (4) and (5) (iii) while the compounds (7), (8) and (10) freeze as amorphous glasses and didn't crystallize even after 6 months (Figure 7 d, e, f). The crystallization behavior suggested difficulties of ordering from molten state, probably because of the highly disorder introduced by the aliphatic chain and noncoplanar arrangement of the oxyphenyl unit to the phenothiazine fragment. On the other hand, the ordering from the glassy state led to continuous crystalline films, without cracks, an important advantage for real world applications [50].

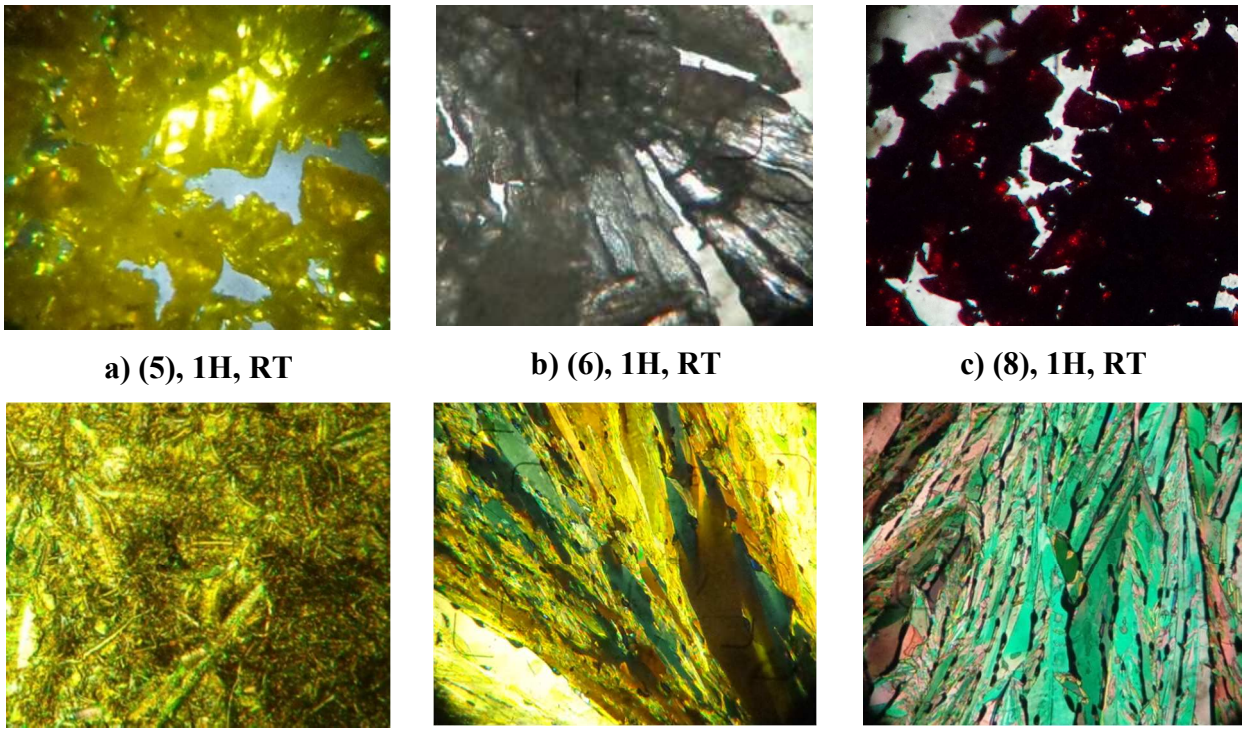

a) (5), 1H, RT **b) (6), 1H, RT** **c) (8), 1H, RT**

d) (5), 1C, RT **e) (6), 1C, 120 ^{o}C** **f) (9), 1C, 197 ^{o}C**

Figure 7. POM images (magnification 200x, C: cooling; H: heating)

Photophysical properties

The UV-vis absorption behavior brings information related to the conjugation degree of the molecules, the absorption capability and allows the estimation of the optical band gap between the HOMO and LUMO levels. As can be seen in Figure 8, all the compounds have an absorption maximum around 260 nm corresponding to the spin allowed π-π* benzenoid transitions of the local aromatic units and a broad absorption band with the maximum between 322 and 343 nm attributed to the localized conjugated skeleton formed by the phenothiazine donor (D) – acceptor (A) framework. In addition, the dyes containing formyl or cyanoacrylic acid unit exhibited a supplementary absorption band with maximum around 400 and 450 nm, respectively, attributed to the intramolecular charge transfer (ICT) from the central electron-donor phenothiazine to the strong electron-acceptor formyl or cyanoacrylic moiety, respectively [30]. This band appeared only as a weak shoulder for the other dyes, related to the weaker electron-acceptor character of the bromine or dimer formation between carboxylic units [51, 52]. The superior absorbance and the stronger bathocromic shifting of the ICT band of the cyanoacrylic dye is associated with (i) the higher electron-acceptor capability of the cyanoacrylic moieties compared to the other electron-acceptor units, and (ii) the presence of the vinyl bond as a π-bridge that allows the charge separation [53].

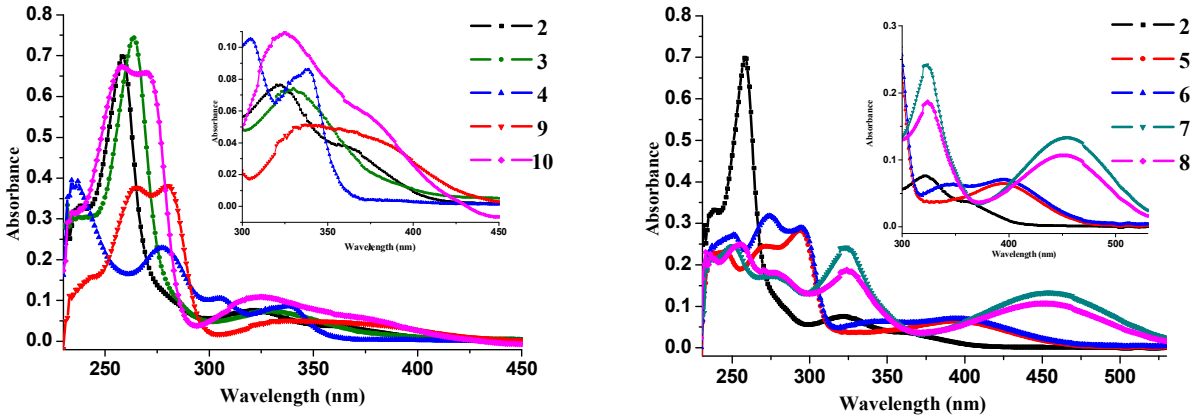

Figure 8. UV-vis absorption spectra, in THF solutions (10^{-5}M) (the inset represents the magnification of the absorption domain over 300 nm)

Concerning the other absorption bands, one can be observed that the formyl containing dyes exhibited the most important bathocromic shift attributed to the strongest electron

delocalization originating from the planar structure and π-π interactions as was proved by the X-ray diffraction. The bromine containing dye (3) also showed a slight bathocromic shift compared to the parent molecule (2), indicating that the electron-withdrawing effect of the bromine was prevalent over its mesomeric electron-donating effect. In the case of the dyes containing bromine as the second substituent (4, 6, 8, 10), no significant effect upon absorption position was observed, according with the weak conjugation between the bromine atom and the phenothiazine core. The absorption parameters attributed to the localized conjugated skeleton formed by donor-acceptor framework are given in Table 1.

Table 1. The absorption parameters attributed to the localized conjugated chromophore

Code	**2**	**3**	**4**	**5**	**6**	**7**	**8**	**9**	**10**
λ_{max}/ λ_{onset} nm)	322/ 404	329/ 372	338/ 365	342/ 460	342/ 467	326/ 530	326/ 531	333/ 433	335/ 441
E_g(eV)	3.85/ 3.06	3.76/ 3.33	3.66/ 3.39	3.62/ 2.69	3.62/ 2.65	3.82/ 2.33	3.82/ 2.33	3.65/ 2.86	3.67/ 2.81

$\lambda_{max}/\lambda_{onset}$: wavelength of absorption maximum / wavelength of absorption edge; *Eg*: energy band gap calculated for the absorption maximum of the peak and for the absorption edge.

The photoluminescence spectra were registered by exciting dye solutions with light of different wavenumber corresponding to the absorption maxima of each dye. All the dyes were luminescent even under day light, the emission color shifted from UV to orange along with the increment of the electron-acceptor capability of the substituent (Figure 9). Thus, the color of the emited light was blue for the phenothiazine core (2), and the bromine (3 and 4) and carboxylic derivatives (9 and 10); green for the formyl derivatives (5 and 6); and orange for the cyanoacrylic derivatives (7 and 8). Since the emission wavelength is controlled by the conjugation length, the dramatic red shifting of the emission maxima (around 200 nm) is explained by the considerable differences between the electron-withdrawing strengths of the acceptor groups.

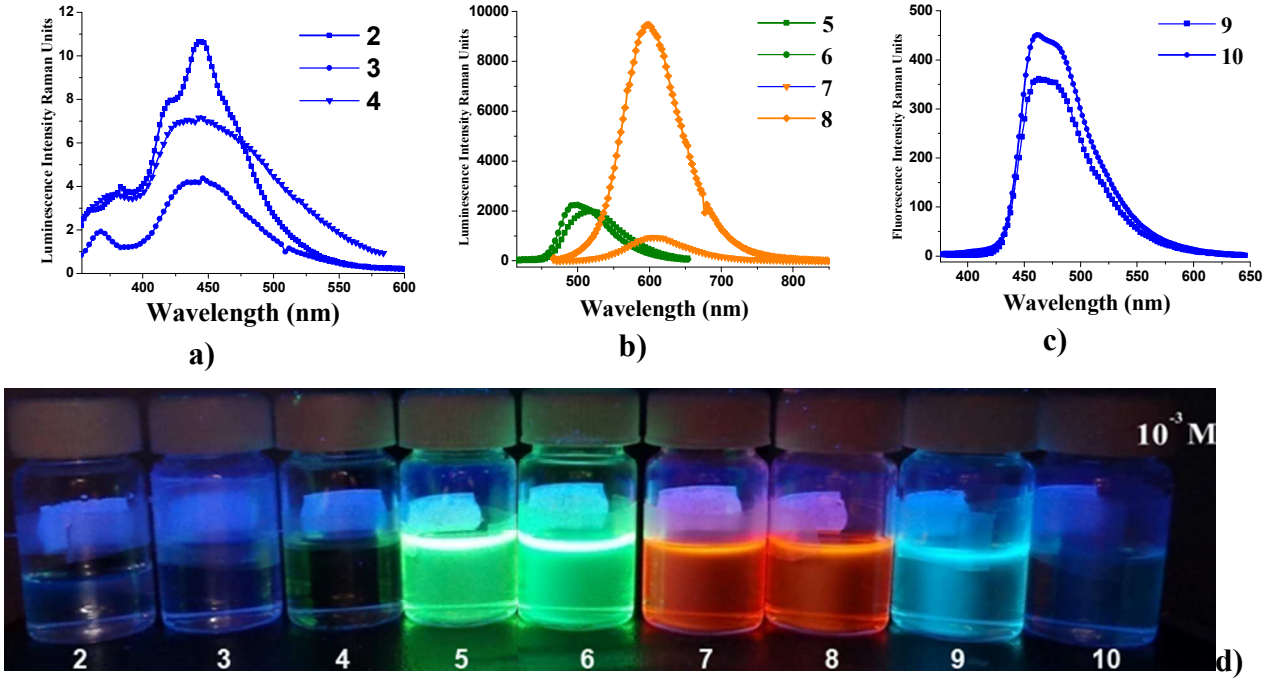

Figure 9. Photoluminescence spectra of the studied dye solutions (THF, 10^{-5}M) (a, b, c) and their luminescence under illumination with UV light (d)

Comparing the emission maxima of the bromine containing compounds (4, 6, 8, 10) with their counterparts without bromine (3, 5, 7, 9), a slight blue shift trend of the emission maxima was observed (Table 2s). This feature was also evident when compared the phenothiazine core (2) with bromine containing dye (3). Considering the weak electron-withdrawing effect of the bromine this blue shifting was attributed to the weakening of the electron-donating ability of the phenothiazine, as was evidenced for other bromine derivatives [54].

To proper compare the dyes emission ability, the fluorescence spectra were registered on solutions of similar molar concentration and their intensity was calibrated using the Raman scatter peak of water [55]. As can be seen in Figure 9a, b. c, the emission intensity increased as the electron-withdrawing ability of the acceptor group increased, following the same trend as the red shifting of the emission color, suggesting that conjugation strength influences the emission intensity, too. Most probably, the explanation for this behavior is given by the reduced amount of non-radiative decay *via* rotational moving and conformational change, as the conjugation strength increases [56].

The increased luminescence is also reflected in the quantum yield values. As can be seen in Table 2, the absolute quantum yield in acetonitrile solution was low for the phenothiazine core (2), and mono-bromine derivative (3), but progressively increased as the electron-acceptor ability of the substituent moiety became higher, reaching up to 71%. Remarkably, the introduction of the bromine as second substituent enhances the quantum yield more than twice. Taking into consideration the weak influence of the bromine upon the absorption, its drastic influence on emission could be attributed to its ability to promote singlet-triplet conversion by enhancing spin-orbit coupling between the excited state electrons and massive nucleus of bromine atoms, which effective busted the quantum yield [44-46]. Another important observation was the good agreement between the luminescence intensity expressed in Raman units and the absolute quantum yield, once again confirming the reliability of calibration using the Raman scatter peak of water [55].

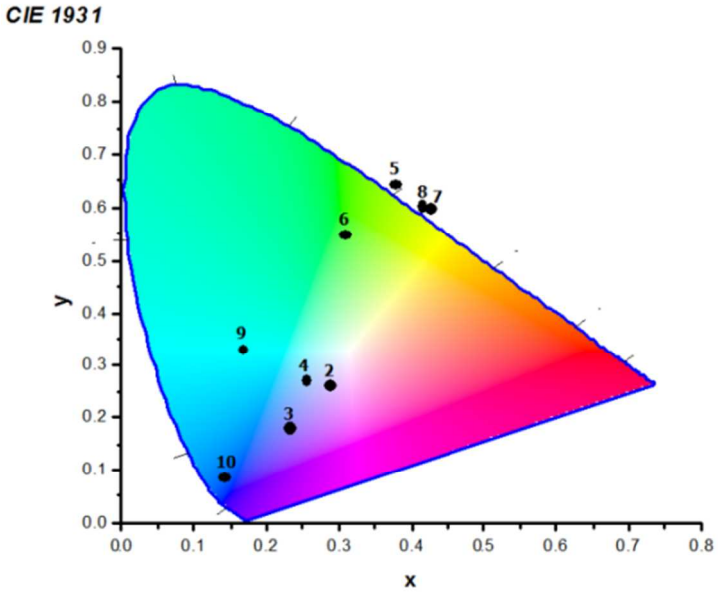

Figure 10. The chromaticity diagram of the dyes

To proper appreciate the chromatic perception of the human eye on the light color of the dye emission, their chromaticity diagram was registered according to available CIE-1931 standard (Figure 10). The chromaticity coordinates from the dye molecules showed the photoluminescence emission colors spanned between blue and yellow visible regions. The (5), (7) and (8) dyes were located on the peripheral zone of the green and yellow region, respectively, indicating emission of pure and fully saturated color, while the (10) dye was located in the blue

region, close to the peripheral zone corresponding to a high color purity of 93 %. The chromaticity coordinates of emission and color purity degree of the studied dyes are summarized in Table 2.

Table 2. Photophysical characteristics of the studied dyes

Code	**2**	**3**	**4**	**5**	**6**	**7**	**8**	**9**	**10**
Stokes shift	122	103	106	148	154	280	272	129	126
η^1%	3.5	3.1	8.5	24.5	66.4	35.5	71.0	29.3	7.8
X^2	0.28	0.23	0.25	0.37	0.30	0.42	0.41	0.16	0.16
Y^3	0.26	0.18	0.27	0.64	0.54	0.59	0.60	0.29	0.33
PC^4(%)	26	52	37	100	59	100	100	66	93
CL^5	purple	blue	Green-bluish	green-yellowish	green-yellowish	yellow green	yellow green	green bluish	green-bluish

[1] absolute quantum yield determined by exciting with light wavenumber corresponding to the absorption maxima of the localized conjugated skeleton formed by donor-acceptor framework; [2, 3] chromaticity coordinates; [4]PC: color purity of emitted light; [5] CL: the color of emitted light

The Stokes shift values were comprised between 49 and 280 nm, resulting in an insignificant overlapping between the absorption and emission profiles, meaning that losses of the emitted photons by re-absorption phenomena were not possible. This is an important feature for multichannel imaging in biochemical applications [57].

Electrochemical behavior

Cyclic voltammetry (CV) of the studied compounds was performed in order to investigate their redox behavior and to further understand their electronic structure. A special concern on the influence of building blocks upon the electronic structure of the dyes and their electrochemical properties was followed, thus allowing assessing their potential as optoelectronic materials. The electrochemical data of the synthesized phenothiazine dyes are collected in Table 3.

Table 3. Electrochemical data of phenothiazine derivatives 2-10

CODE	2	3	4	5	6	7	8	9	10
E_{onset}^{ox} (V)	0.645	0.740	0.802	0.830	0.888	0.743	0.852	0.776	0.845
E_{pa} (V)	0.814, 1.634	0.953, 1.686	0.949, 1.619	1.016, 1.730	1.068, 1.754	0.964, 1.777, -1.400	1.040, 1.307, 1.641, -1.375	0.966, -1.472	0.979, 1.732
E_{onset}^{red} (V)	-0.593	-0.640	-0.647	-0.654	-0.603	-0.895	-0.918	-0.611	-0.636
E_{pc} (V)	0.640, -1.277	0.711, -1.337	0.815, 0.555, -1.186	1.394, 0.807, -1.262, -1.550	0.852, 0.564, -1.300	0.757, -1.690	0.887, 0.692, -1.564	0.677, -1.417	0.677, 0.802
IP (eV) HOMO	4.99	5.09	5.15	5.18	5.24	5.09	5.20	5.13	5.19
EA (eV) LUMO	3.76	3.71	3.70	3.70	3.75	3.45	3.43	3.74	3.71
E_g (eV)	1.23	1.38	1.45	1.48	1.49	1.64	1.77	1.39	1.48

E_{onset}^{ox} - oxidation onset potential; E_{onset}^{red} - reduction onset potential, E_{pa} - anodic peak potential; E_{pc} - cathodic peak potential; E_{HOMO} - the HOMO energy level, E_{LUMO} - the LUMO energy level, E_g - energy gap measured from electrochemical data according to the E_{onset}

All the phenothiazine dyes electrochemically oxidize, indicating their *p*-type doping capability and hole transport characteristics. The parent phenothiazine molecule (2), revealed two oxidation peaks at the anodic peak potentials E_{pa1} = 0.814 V and E_{pa2} = 1.634 V *vs*. SCE, respectively, and one reduction peak at the cathodic peak potential E_{pc} = 0.640 V *vs*. SCE. The two oxidation peaks were related to the formation of radical cation and dication species. The first oxidation of the phenothiazine led to the formation of the radical cation species at the nitrogen center, which further converted to the dication species by oxidation at the free electron pair of the sulfur atom [58, 59]. The anodic scan evidenced that the first phenothiazine-centered oxidation potential could be fine-tuned using suitable electron-acceptor substituents, the anodic peak potential (E_{pa}) values ranging from 0.814 to 1.068 V *vs*. SCE. A closer inspection of the electrochemical behavior of the mono-substituted phenothiazine dyes (3), (5), (7) and (9) revealed the first reversible one-electron oxidation was shifted to higher values (E_{pa1} = 0.953, 1.016, 0.964 and 0.966 V *vs*. SCE, respectively) relative to that of the phenothiazine parent

molecule (2) (E_{pa1} = 0.814 V *vs*. SCE) as a consequence of the electron-withdrawing effect of the substituents (Figure 11).

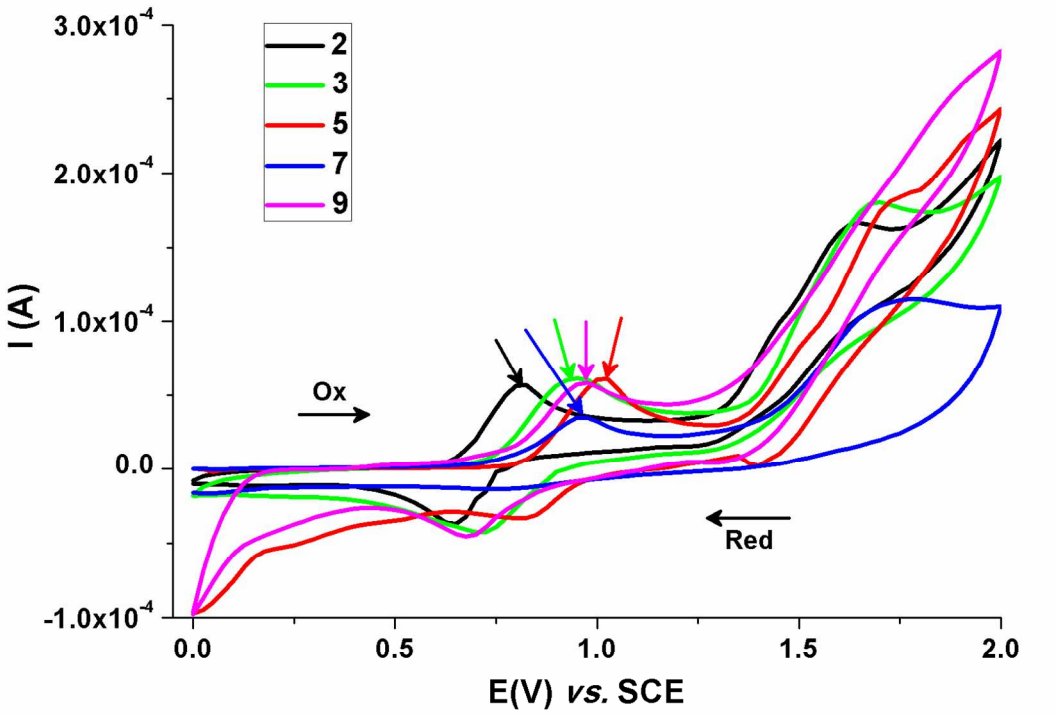

Figure 11. CV diagrams of phenothiazine (2) and its electron-withdrawing moieties monosubstituted analogous, (3), (5), (7) and (9), in the positive region

As a matter of fact, the electron-withdrawing substituents have an active contribution in the formation of a push-pull system, by accepting the electrons from the electron-donating phenothiazine. Hence, the electron density on phenothiazine core should decrease once the electron-acceptor character of the substituents increases, and oxidation should become more difficult. Among the used substituents, cyanoacrylic acid moiety has the strongest electron-acceptor character and bromine the lowest one. Therefore it was expected as the cyanoacrylic acid-substituted phenothiazine (7) to be the most difficult oxidized. Instead, the formyl-substituted phenothiazine dye (5) exhibited the most anodically shifted peak (Figure 11). In close correlation with its X-ray molecular structure presented in figure 1 and UV-Vis absorption behavior mirrored in figure 8, such a feature was attributed to the better strength electronic conjugation of the dye (5) (in which the phenothiazine donor was directly connected with the formyl acceptor) that prevailed over the electron-withdrawing character. On the other hand, the

ability of the carboxylic acid in (9) to promote H-bonding (see the crystal motif) and to polarize is a direct function of the electronic properties and bonding order of the atoms that make up the COOH moiety. Thus, the electronic density is "pulled" from the hydroxyl hydrogen through the conjugated carboxyl group and, consequently, this group could exert a lower electron-accepting effect in (9) compared to the aldehyde unit in (5), explaining its easier oxidation. From all investigated substituents only the formyl and cyanoacrylic groups hampered the reversibility of the first mono-electronic oxidation process of the phenothiazine, probably due to the low stability of the intermediate radical cation – affected by the electron-withdrawing mesomeric effect.

When bromine atom was introduced as the second substituent, the phenothiazine dyes (4), (6), (8) and (10) became harder to be oxidized, indicating a decreased electron density on the phenothiazine core compared to the mono-substituted analogues (Figure 12). This is in agreement with the predominance of the negative inductive effect of the bromine atom over its positive mesomeric effect, the bromine atom exerting an electron-withdrawing capability, as was confirmed by X-ray crystal structure of (4) and (6) and photophysical data of all Br-substituted phenothiazine derivatives. However, its capability to accept electrons appears to be minimal in (4), when the first substituent is a bromine atom also.

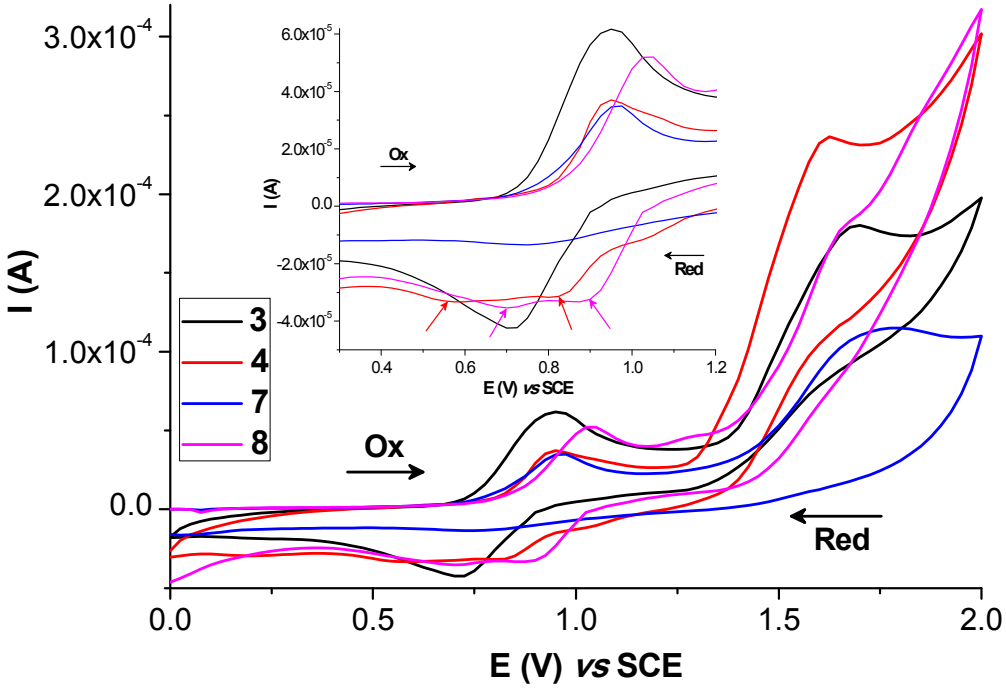

Figure 12. Diagrams of representative mono- and di-substituted phenothiazine dyes, obtained by current sweep in the positive direction

The broad irreversible oxidation wave observed in the potential range from 1.619 to 1.777 V *vs* SCE corresponds to the formation of the highly reactive phenothiazine dications, and it is no longer present for the compound (9). The irreversibility in the oxidation of the dications is most likely due to a following chemical reaction with trace water or the solvent [60]. On the reverse scanning, one reduction process assigned to the reduction of the phenothiazine radical cations occurred at E_{red} from 0.677 to 0.787 V vs. SCE in the case of monosubstituted derivatives (Figure 11). The presence of the bromine as a second substituent caused the appearance of two closely spaced reduction waves attributed to two phenothiazine radical cations, at the peak potentials presented in Table 3 (Figure 12). As the two closely spaced reduction waves were one-electron waves, appeared reasonable to assume that the two identical phenothiazine molecules in the disubstituted derivatives (4, 6, 8 and 10) were not completely electronically decoupled, so that these two waves represented individual one electron reduction of each phenothiazine radical cation at a slightly different potential. The overlapping reduction waves indicated that the two phenothiazine molecules had some molecular orbital interactions the most probably due to the ability of bromine to promote self-assembling through π-π stacking, as X-ray data of (4) and (6) indicated; if the two phenothiazine units should be completely out of plane or orthogonal to one another, a single one-electron reduction wave should be observed like in the case of monosubstituted counterparts, for such a behavior the bromine atom being responsible.

Scanning in the negative direction to -2 V *vs* SCE, all the phenothiazine dyes exhibited reduction waves, in accord with the electron deficient nature of the electron-acceptor units, indicating their *n*-type dopability and electron transport characteristics (Table 3). The most interesting feature was the large reduction peak centered at -1.39 V *vs*. SCE, without a corresponding anodic wave for the parent molecule (2) (Figure 13). It appears that the *N*-substitution of the phenothiazine with hexyloxy-phenyl moiety make this molecule suitable for electrochemical reduction (it can accept electrons). A close look to the crystal structure of (2) shows that two crystallographic equivalent molecules are linked to form dimeric units through C-H···O hydrogen bonding, were the O atom of hexyloxy-pheny unit acts as a proton acceptor. In the light of this finding, it appears that the electron density on O became enough lower as to accept one electron and promote the *n*-doping process of (2). In the electron-withdrawing monsubstituted molecules (3, 5, 7 and 9**)**, the reduction peak potential vary by 0.42 V, between -1.27 and -1.69 V *vs.* SCE, a decreasing being observed as much as the electron delocalization

progressively increased due to the higher electron-accepting capability. When the first bromine substituent was grafted on the phenothiazine core (3), this trend was followed, but it exerted a small influence on the reduction potential. When the bromine was placed as a second substituent (4, 6, 8, 10) it facilitated the reduction of the molecule dyes, being accomplished by the anodically shift of the reduction potential (Figure 13). Such a feature accounts for bromine ability to increase the strength of the push-pull system.

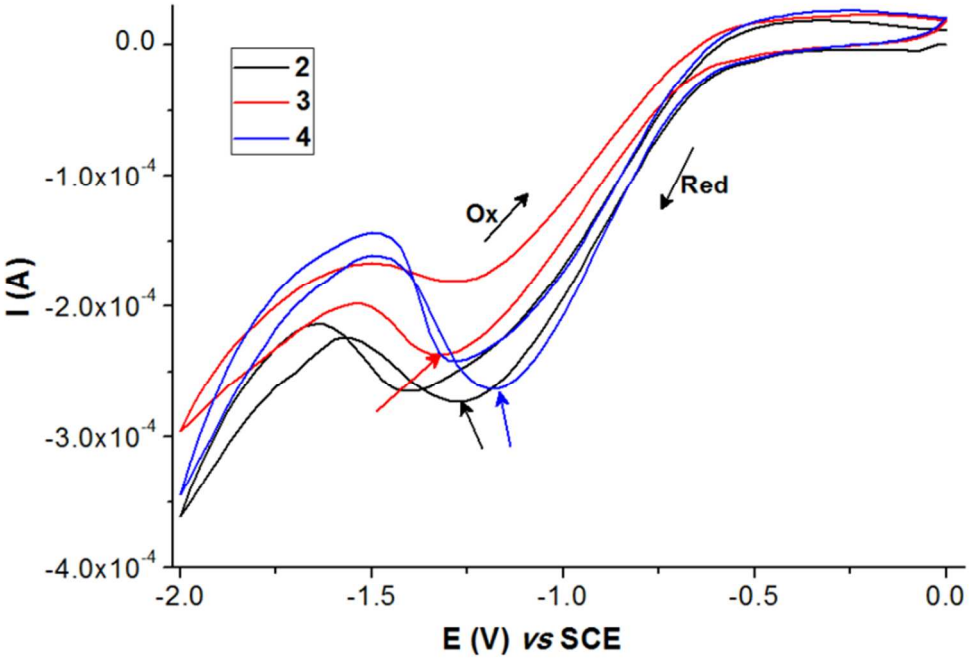

Figure 13. CV diagrams of phenothiazine (2) and its Br-substituted analogous in the negative region

The electron-withdrawing substituents produced peculiar reduction waves. The formyl-substituted phenothiazine (5) displayed two reduction waves (Table 3), the one peaking at -1.55 *vs.* SCE being attributed to the reduction of the aldehyde group, while (7) and (9) showed only one reduction peak at -1.69 and -1.42 V, respectively, being attributed to the formation of radical anions of the electron-withdrawing cyanoacrylic and carboxylic units, respectively (Figure 14). A further oxidation to neutral species of the formed radical anions was observed for both (7) and (9) molecules. A similar trend was noticed for their Br-substituted counterparts, (8) and (9), but at slightly more positive potential values (Table 3).

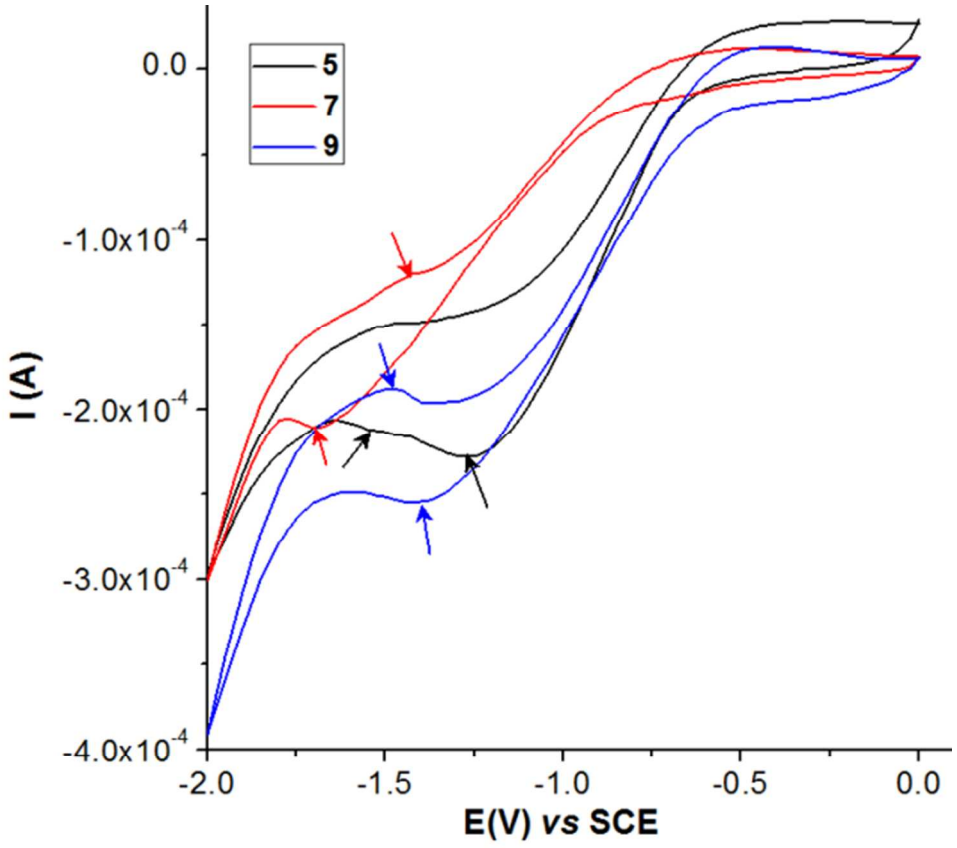

Figure 14. CV diagrams of the phenothiazine derivatives (5), (7), and (9) in the negative region

As a general conclusion, the electrochemical behavior of the compounds under study suggests that *p*- and *n*-type doping to conducting state of these phenothiazine materials is feasible. These systems can therefore be used as electrochemically amphoteric push-pull chromophores that can accept or release electrons at relatively low voltages. For applications in organic light-emitting diodes (OLEDs) or organic field-effect transistors as functional hole- and electron- transport layer this is a beneficial property. Additionally, the highly fluorescent phenothiazine derivatives 5 – 9 could also serve as redox switchable emitters in OLED devices.

Electronic structure

To gain an insight upon the electronic structure of the dyes, the HOMO and LUMO energy levels were calculated based on the assumption that the oxidation process corresponds to the electron removal from HOMO orbitals (ionization potential, IP), and the reduction process corresponds to the electron addition to the LUMO level (electron affinity, EA). Thus, the energy levels of HOMO and LUMO orbitals of the investigated phenothiazine dyes can be estimated *vs.*

zero vacuum level from the onset of the oxidation (E^{ox}_{onset}) and reduction (E^{red}_{onset}) potential *vs* SCE, respectively. The external ferrocene/ferrocenium (F_c/F_c^+) redox standard E_{onset} is 0.45 V versus SCE. Assuming that the HOMO energy for the F_c/F_c^+ standard is 4.80 eV with respect to the zero vacuum level [61], the HOMO and LUMO energy levels and the electrochemical energy band gap (E_g) (in eV) were calculated according to the following equations:

$E_{LUMO} = EA = E^{red}_{onset} + 4.35$; $E_{HOMO} = IP = E^{ox}_{onset} + 4.35$; $E_g = E_{HOMO} - E_{LUMO}$

The values of the HOMO and LUMO energy levels and the energy gap characteristics for the phenothiazine dyes (2-10) calculated from electrochemical data are summarized in Table 3. The EA values varied between 3.43 and 3.76 eV, the highest one being obtained for the parent molecule (2), which does not contain any electron-acceptor substituent on the phenothiazine core. An evident reduction of the LUMO energy (in the absolute value), was noticed for the phenothiazine derivatives containing cyanoacrylic acid substituent (7) and (8), attributed to the increased delocalization of the electrons between donor and acceptor units. Thus, the LUMO level appeared to be mainly located at the electron-withdrawing cyanoacrylic moiety through the π-spacer, giving the strongest donor-acceptor strength. In perfect agreement with foregoing observations, the Br atom decreased the LUMO level to some extent, thus proving ones more its "pull" effect on the phenothiazine core. On the other hand, the IP values ranged between 4.99 and 5.24 eV, a magnification being accomplished as the electron-acceptor capability of the substituent increased, as previously discussed. Using the HOMO energy level of (2) as a reference, it could be observed that the electron-acceptor substituents guided the HOMO energy level to values comparable with well recognized semiconducting polymers as poly(*p*-phenylenevinylene) (5.11) or poly(*p*-phenylene) (5.42 eV) [62].

The band structure of the (1-10) dyes calculated from electrochemical data is depicted in Figure l5. As can be seen, the resulted values for the energy band gap of the phenothiazine dyes (2-9) vary between 1.23 and 1.77 eV. An important disparity was ascertained between the energy band gap values measured by UV-Vis absorption and electrochemical techniques. There is no contradiction between these values, since they refer to distinct processes. The UV-Vis absorption data provide an estimation of the energy difference of the HOMO-LUMO orbitals while the obtained optical band gap is consistent with the energy required to form a tightly-bound exciton. The redox potentials measured by cyclic voltammetry afford the absolute energetic positions of

the HOMO and LUMO levels and the electrochemical or transport band gap depicts the energy required to form free charge carriers [63].

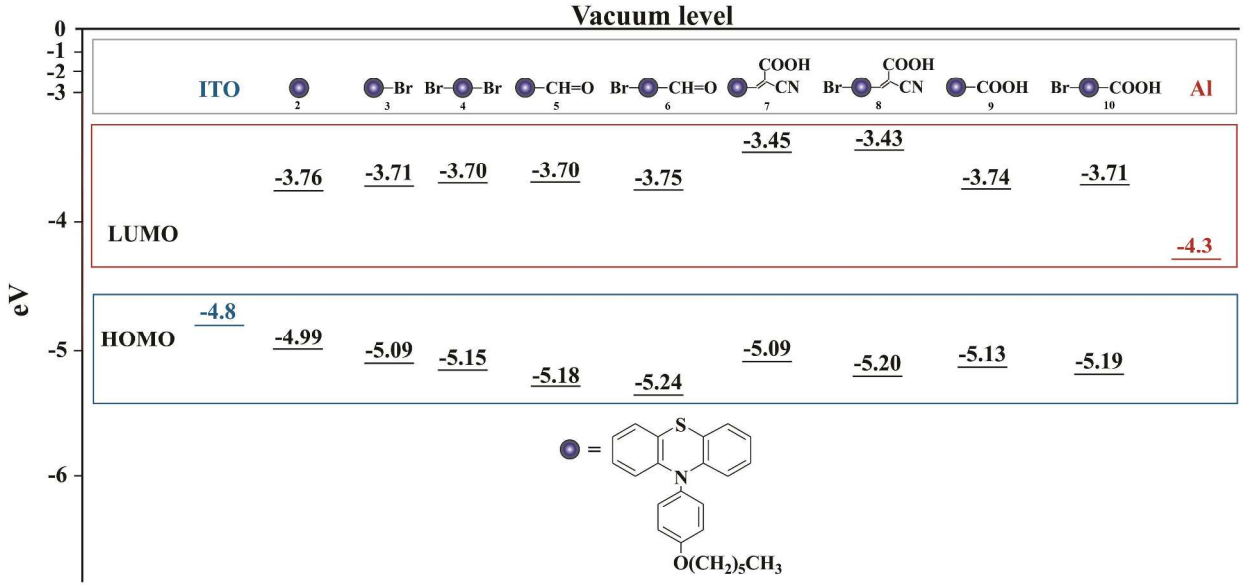

Figure l5. Band diagrams of the phenothiazine dyes 2-10 as evaluated from electrochemical data

The energy barriers between the light-emitting materials and electrodes can be assessed on the basis of the work functions of electrodes and EA and IP of the respective material. Taking into consideration the work function of ITO anode (4.8 eV) and aluminium cathode (4.3 eV), the hole and electron injection barriers, respectively, between the emitting compounds and electrodes can be calculated as ΔE_h = IP - 4.8 (eV) and ΔE_e = 4.3 - EA (eV). Moreover, the difference between the electron and hole injection barriers which give information about the balance in the two injections, can be calculated as (ΔE_e - ΔE_h). The barrier energy values are comprised in Table 4.

Table 4. The barrier energies of phenothiazine derivatives 2 - 10

Code	2	3	4	5	6	7	8	9	10
ΔE_h	0.19	0.29	0.35	0.38	0.44	0.29	0.40	0.33	0.39
ΔE_e	0.54	0.59	0.6	0.6	0.55	0.85	0.87	0.56	0.59
ΔE_e-ΔE_h	0.35	0.3	0.25	0.22	0.11	0.56	0.47	0.23	0.20

ΔE_h - barrier energy for hole injection from ITO to the dye; ΔE_e - barrier energy for the electron injection from Al to the dye; ΔE_e - ΔE_h - the difference of barrier energy between electron and hole injection to the dye.

Both hole and electron injection barriers had small values indicating an easier injection of both charge carriers. Lower difference between hole and electron injection barriers (ΔE_e - ΔE_h) means improved injection balance of electrons and holes from the cathode and anode, respectively. It was evident that introduction of the bromine increased the hole injection barrier in a similar manner as all the other electron-acceptor units do. Meanwhile, the bromine exerted a slightly influence on the electron injection barrier, except the case of the cyanoacrylate derivatives (7, 8) when it considerably increased due to the higher electron delocalization encountered in these systems between the donor and acceptor units through the vinyl π- bridge. However, the barrier energy differences (ΔE_e - ΔE_h) of these phenothiazine dyes were very low, comparable to that of the semiconducting light emitting polymers used as electron- and hole transporting light-emitting layers in OLED devices [64].

Conclusions

A series of nine dyes built by functionalization of a donor phenothiazine core with heavy bromine and/or carbonyl containing acceptors have been successfully synthesized and their crystallographic, thermotropic, photophysical and electrochemical peculiarities were investigated in detail.

The crystallographic study demonstrated that phenothiazine substituents play a decisive role on the morphological peculiarities, leading to different packing motifs as dimers, tetramer clusters, supramolecular ribbons or even linear arrays with unusual phenothiazine π-π stacking. It was evidenced that the direct connection of the formyl group to the phenothiazine unit lead to a high planarization and consequently high electron delocalization and π-π stacking interactions, indicating this combination of building blocks as a potential strategy in designing compounds for applications which claim high charge carrier mobility. The introduction of the bromine as second substituent appeared to favor even stronger π-π stacking interactions.

The direct connection of the acceptor units to the phenothiazine donor led to a lower band gap, while the presence of a π bridge facilitated the charge separation resulting in a strong intramolecular charge transfer and huge Stokes shift of about 280 nm, which account for multichannel imaging applications.

The use of acceptor substituents with various electron-withdrawing strength produced drastic shifting of the color of emitted light from UV to orange.

While the introduction of the bromine as a primary substituent of the phenothiazine core had a low influence upon the emission intensity, its effect dramatically changed when it was introduced as a second substituent in addition to a strong electron-acceptor one, enhancing twice the quantum yield. The cyclovoltametry measurements indicated that bromine promoted some molecular orbital interactions which could explain its drastic effect on the luminescence efficiency. Moreover, the bromine proved ability to increase the strength of the push-pull system by favoring the reduction process and thus *p*-type conduction.

All the studied compounds are promising as *p*- and *n*-type materials and have very good electronic characteristics which recommend them as ambipolar luminescent materials for optoelectronic applications.

Supporting Information

The Supporting Information is available free of charge on the ACS Publications website. Data for synthesis and structural characterization; ^{1}H-NMR and ^{13}C-NMR spectra; Crystallographic data, details of data collection and structure refinement parameters; Optical parameters.

Acknowledgements

The research leading to these results has received funding from the Romanian National Authority for Scientific Research, MEN – UEFISCDI, project number PN-II-PT-PCCA-2013-4-1861 (contract number 272/2014) and from Horizon 2020 ERA Chairs Projects, no: 667387: SupraChemLab Laboratory of Supramolecular Chemistry for Adaptive Delivery Systems ERA Chair initiative.

Notes and references

1 Bures, F. *RSC Adv*. **2014**, *4*, 58826–58851.

2 Iqbal, Z.; Wu, W.Q.; Huang, Z.S.; Wang, L.Y.; Kuang, D.B.; Meier, H.; Cao, D. *Dyes Pigments* **2016**, 124, 63–71.

3 Wan, Z.Q.; Jia, C.Y.; Wang, Y.; Luo, J. S.; Yao, X.J. *Organic Electronics* **2015**, *27*, 107–113.

4 Sharma, G. D.; Reddy, M. A.; Ramana, D. V.; Chandrasekharam, M. *RSC Adv*. **2014**, *2*, 33279–33285.

5 Yang, L.; Feng, J. K.; Ren, A. M. *J. Org. Chem*. **2005**, *70*, 5987–5996.

6 Lee, M.; Park, J. E.; Park, C.; Choi, H. C. *Langmuir* **2013**, *29*, 9967–9971.

7 Zhu, M.; Luo, H.; Wang, L.; Yu, G.; Liu, Y. Q. *Acta Chimica Sinica* **2012**, *70*, 1599–1603.

8 Hwang, D. H.; Kim, S. K.; Park, M. J.; Lee, J. H.; Koo, B. W.; Kang, I. N.; Kim S. H.; Zyung, T. *Chem. Mat*. **2004**, *16*, 1298-1303.

9 Ramachandran, E.; Dhamodharan, R. *J. Mater. Chem. C* **2015**, *3*, 8642-8648.

10 Daub, J.; Engl, R.; Kurzawa, J.; Miller, S. E.; Schneider, S.; Stockmann A.; Wasielewski, M. R. *J. Phys. Chem. A* **2001**, *105*, 5655–5665.

11 Sun, J.; Jiang, H. J.; Zhang, J. L.; Tao Y.; Chen, R. F. *New J. Chem.* **2013**, *37*, 977–985.

12 Ahn, S.; Cha, Y. B.; Kim, M.; Ahn K. H.; Kim, Y. C. *Synthetic Met*. **2015**, *199*, 8–13.

13 Tanaka, H.; Shizu, K.; Nakanotani H.; Aldachi, C. *J. Phys. Chem. C* **2014**, *118*, 15985–15994.

14 Park, Y.; Kim, B.; Lee, C.; Hyun, A.; Jang, S.; Lee, J. H.; Gal, Y. S.; Kim, T. H.; Kim K. S.; Park, J. *J. Phys. Chem. C* **2011**, *115*, 4843–4850.

15 Ananthakrishnan, S. J.; Varathan, E.; Subramanian, V.; Somanathan N.; Mandal, A. B. *J. Phys. Chem. C* **2014**, *118*, 28084–28094.

16 Tang, Z. B.; Sun, X. X.; Miao L. P.; Shen, H. Y. *Adv. Mater. Res*. **2014**, *989–994*, 284–287.

17 Sun, Q.; Mu, L.; Zeng, X.; Zhao, J.; Yamato T.; Zhang, J. *Sci. China Chem*. **2015**, *58*, 539–544.

18 Petran, A.; Terec, A.; Bogdan, E.; Soran, A.; Lakatos E.; Grosu, I. *Tetrahedron* **2014**, *70*, 6803–6809.

19 Jahnke, A. C.; Spulber, M.; Neuburger, M.; Palivan, C. G.; Wenger, O. S. *Chem. Commun*. **2014**, *50*, 10883–10886.

20 Zabulica, A.; Balan, M.; Belei, D.; Sava, M.; Simionescu B. C.; Marin, L. *Dyes Pigments* **2013**, *96*, 686–698.

21 Bende, A.; Grosu, I.; Turcu, I. *J. Phys. Chem. A* **2010**, *114*, 12479–12489.

22 Sun, D.; Rosokha, S. V.; Kochi, J. K. *J. Am. Chem. Soc*. **2004**, *126*, 1388–1401.

23 Wang, H.; Xu, W.; Zhang, B.; Xiao, W.; Wu, H. *Acta Cryst. E* **2008**, *64*, o2458.

24 Yu, D-H.; Wang, J.-Q.; Kong, L.; Liu, Z.-D. *Acta Cryst.* E **2011**, *67*, o3344.

25 Wang, H.; Xu, W.; Zhang, B., *J. Chem. Cryst.* **2012**, *42*, 846–850.

26 Bolton, O.; Lee, K.; Kim, H. J.; Lin K. Y.; Kim, J. *Nat. Chem*. **2011**, *3*, 205–210.

27 Zhang, Y.; Wang, J. H.; Zheng J.; Li, D. *Chem. Commun*. **2015**, *51*, 6350–6353.

28 Chen, C. J.; Liao, J. Y.; Chi, Z. J.; Xu, B. J.; Zhang, X. Q.; Kuang, D. B.; Zhang, Y.; Liu S.; Xu, J. *J. Mat. Chem*. **2012**, *22*, 8994–9005.

29 Iqbal, Z.; Wu, W. Q.; Kuang, D. B.; Wang, L.; Meier, H.; Cao, D. *Dyes Pigments* **2013**, *96*, 722–731.

30 Yamanishi, H.; Tomita, I.; Ohta, K.; Endo, T. *Mol. Cryst. Liq. Cryst*. **2001**, *369*, 47–61.

31 Wang, H.; Xu, W.; Zhang, B. *J. Chem. Crystallogr*. **2012**, *42*, 846–848.

32 Qian, X.; Chang, W. Y.; Zhu, Y. Z.; Wang, S. S.; Pan, B.; Lu L.; Zheng, J. Y. *RSC Adv*. **2015**, *5*, 47422–47428.

33 The synthesis of the acid derivative by aldehyde oxidation in the presence of *t*-BuOK is first time reported by us here.

34 Iosip, M. D.; Destri, S.; Pasini, M.; Porzio, W.; Pernstich, K. P.; Batlogg, B. *Synthetic Met*. **2004**, *146*, 251–257.

35 CrysAlis RED, Oxford Diffraction Ltd., Version 1.171.36.32, 2003.

36 Dolomanov, O. V.; Bourhis, L. J.; Gildea, R. J.; Howard J. A. K.; Puschmann, H. *J. Appl. Cryst*. **2009**, *42*, 339–341.

37 Sheldrick, G. M. *Acta Cryst*. **2008**, *A64*, 112–122.

38 Elkassih, S. A.; Sista, P.; Magurudeniya, H. D.; Papadimitratos, A.; Zakhidov, A. A.; Biewer M. C.; Stefan, M. C. *Macromol. Chem. Phys*. **2013**, *214*, 572–577.

39 Rajakumar, P.; Satheeshkumar, C.; Ravivarma, M.; Ganesan S.; Maruthamuthu, P. *J. Mat. Chem. A* **2013**, *1*, 13941–13948.

40 Kong, X. X.; Kulkarni A. P.; Jenekhe, S. A. *Macromolecules* **2003**, *36*, 8992–8999.

41 Belei, D.; Dumea, C.; Bicu E.; Marin, L. *RSC Adv.* **2015**, *5*, 8849–8858.

42 Kim, S. H.; Sakong, C.; Chang, J. B.; Kim, B.; Ko, M. J.; Kim, D. H.; Hong K. S.; Kim, J. P. *Dyes Pigments* **2013**, *97*, 262–271.

43 Xue, P.; Yao, B.; Liu, X.; Sun, J.; Gong, P.; Zhang, Z.; Qian, C.; Zhang, Y.; Lu, R. *J. Mater. Chem. C* **2015**, *3*, 1018–1025.

44 Mukherjee, S.; Thilagar, P. *Chem. Commun*. **2015**, *51*, 10988–11003.

45 Xu, J. J.; Takai, A.; Kobayashi, Y.; Takeuchi, M. *Chem. Commun*. **2013**, *49*, 8447–8449.

46 Ventura, B.; Bertocco, A.; Braga, D.; Catalano, L.; d'Agostino, S.; Grepioni F.; Taddei, P. *J. Phys. Chem. C* **2014**, *118*, 18646–18658.

47 Havlas, Z.; Michl, J. *J. Am. Chem. Soc.* **2002**, *124*, 5606-5607.

48 Pavan, M. S.; Pal, R.; Nagarajan, K.; Row, T. N. G. *Cryst. Growth Des*. **2014**, *14*, 5477–5485.

49 Awwadi, F. F.; Willett, R. D.; Twamley, B.; Turnbull, M. M.; Landee, C. P. *Cryst. Growth Des*. **2015**, *15*, 3746–3754.

50 Zhang, G.; Sun, J.; Xue, P.; Zhang, Z.; Gong, P.; Peng J.; Lu, R. *J. Mat. Chem*. **2015**, *3*, 2925–2932.

51 Perepichka, D. F.; Bryce, M. R.; Batsanov, A. S.; Howard, J. A.; Cuello, A. O.; Gray M.; Rotello, V. M. *J. Org. Chem*. **2001**, *66*, 4517–4524.

52 Kuhnt, C.; Karnahl, M.; Rau, S.; Schmitt, M.; Dietzek B.; Popp, J. *Chem. Phys. Lett*. **2011**, *516*, 45–50.

53 Ricks, A. B.; Solomon, G. C.; Colvin, M. T.; Scott, A. M.; Chen, K.; Ratner M. A.; Wasielewski, M. R. *J. Am. Chem. Soc*. **2010**, *132*, 15427–15434.

54 Xue, P.; Yao, B.; Sun, J.; Xu, Q.; Chen, P.; Zhang, Z.; Lu, R. *J. Mater. Chem. C* 2014, *2*, 3942–3950.

55 Lawaetz, J.; Stedman, C. A. *Appl. Spectrosc*. **2009**, *63*, 936–940.

56 Hong, Y.; Lam, J. W. Y.; Tang, B. Z. *Chem. Soc. Rev*. **2011**, *40*, 5361–5388.

57 Horvath, P.; Sebej, P.; Solomek, T.; Klan, P. *J. Org. Chem*. **2015**, *80*, 1299–1311.

58 Clarke, D.; Gilbert, B.C.; Hanson, P.; Kirk, C.M. *J. Chem. Soc., Perkin Trans.* **1978***, 2*, 1103–1110.

59 Hayen, H.; Karst, U. *Anal. Chem*. **2003**, *75*, 4833–4840.

60 Perichon, J. In *Encyclopedia of Electrochemistry of the Elements*; Bard, A. J., Lund, H., Eds.; Marcel Dekker: New York, 1978; Vol. 11, Chapter 1, pp 132–135.

61 Pomrnerehne, J.; Vestweber, H.; Gun, W.; Muhrt, R.E.; Bassler, H.; Porsch, M.; Daub, J. *Adv. Mater.* **1995**, *7*, 551–554.

62 Cervini, R.; Li, X.; Spencer, G. W. C.; Holmes, A. B.; Moratti S. C.; Friend, R. H. *Synthetic Met*. **1997**, *84*, 359–360.

63 Takeda, Y.; Andrew, T. L.; Lobez, J. M.; Mork A. J.; Swager, T. M. *Angew. Chem*. **2012**, *124*, 9176–9180.

64 Akcelrud, L. *Prog. Polym. Sci*. **2003**, *28*, 875–962.

For Table of Contents Use Only

Structure-directed functional properties of phenothiazine brominated dyes. Morphology, photophysical and electrochemical properties

Andrei Bejan, Sergiu Shova, Mariana Dana Damaceanu, Bogdan C. Simionescu and Luminita Marin*

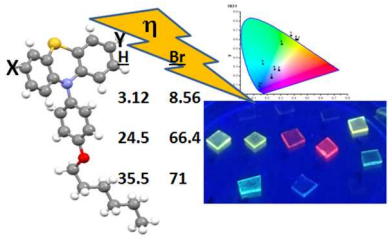

A systematic study of a series of nine D-A dyes based on a phenothiazine core functionalized with a heavy bromine atom and/or various carbonyl containing acceptors proved the decisive role played by the substituents on the packing peculiarities and thermotropic, photophysical and electrochemical behavior.